Research Article

A Simple Mathematical Model for Extreme Flood Actions on Superstructures of Coastal Bridges

George T. Michaltsos[1]* ID, Dimitrios S. Sophianopoulos[2] ID, Theodor G. Konstantakopoulos[2]

[1]School of Civil Engineering, National Technical University of Athens, 15875 Athens, Greece
[2]Department of Civil Engineering, University of Thessaly, 38334 Volos, Greece
 Email: michalts@central.ntua.gr

Abstract: Coastal bridges may be strongly affected by extreme flood actions (mainly tsunamis), which may be caused by earthquakes, volcanic eruptions, and other underwater explosions (including detonations, landslides, glaciers calvings, meteorite impacts, and other disturbances) above or below water. A simple mathematical model for analysis, processing, and easy yet effective mathematical manipulation is proposed and studied with the aid of simple principles of hydraulics, for investigating the aforementioned effects, in order to avoid rigorous analyses using ocean and coastal engineering. The main idea is based on the investigation of a water vein squirted from a height with a constant horizontal initial velocity, and the analysis of the critical wave in water veins. The results obtained, including the dynamics of deck superstructures and safety issues, reveal the critical situation for avoiding the devastating phenomena of rocking, overturning, and shifting in exemplary small and large coastal bridges. It is found that larger (longer) bridges exhibit acceptable deformations, contrary to smaller ones, while the overturning phenomenon seems to be the most critical one for both types of bridges.

Keywords: coastal bridges, rocking, overturning shifting, flood actions, dynamics of bridges

1. Introduction

Coastal bridges near shores of shallow waters or bridges connecting the mainland with islands are constructions common today. These bridges are usually designed for normal conditions. However, there are cases of extreme waves due to tsunamis, which are generated by the displacement of water by a large event, and race across the sea at up to 500 miles (805 kilometers) an hour - about as fast as a jet airplane. At that pace, they can cross the entire expanse of the Pacific Ocean in less than a day. Their long wavelengths mean that they lose very little energy along the way.

So, in order not to impede navigation, long-span bridges that connect the mainland coast with islands have a deck built quite high above sea level. Therefore, the tsunami waves cannot affect the deck of the bridge but probably the pylons, which usually have the strength to resist the applied forces. Coastal bridges, on the other hand, have decks that are constructed a short distance from the water level. This distance under special conditions, for example, storms, can be decreased, allowing water to approach the bottom or top surface of the deck.

The usual protection of bridge decks against external load forces is by making use and benefiting from their dead

weight and the application of some rather weak connections. The above are incapable of withstanding the loads due to strong storms or tsunamis.

The following two examples are characteristic:

After the earthquake of March 27, 1964, in the Gulf of Alaska, and the developed extreme floods, the steel trusses of the Copper River and Northwestern Railroad Bridge near Round Island were shifted from one-third to two-thirds of a meter (Figure 1a).

In the earthquake of February 4, 1976, in Guatemala, three central spans of the Agua Caliente Bridge collapsed on the road to the Atlantic Ocean. Both ground shaking and extreme floods contributed to this collapse (Figure 1b).

Several papers have been reported in the literature, dealing with the rocking, overturning, and shifting problems in bridges due mainly to earthquake and extreme flood actions. Zerva [1] evaluated the response of continuous two- and three-span beams of various lengths subjected to spatially varying seismic ground motion. Using a stochastic representation of this motion as input at the supports, sensitivity analyses of the response with respect to the degree of correlation between the support motions were performed. It was found that the commonly used assumption of equal support motion is questionable. Moreover, the effect of non-uniform seismic excitation on short bridges was studied by Price and Eberhard [2]; the authors developed a method that relies on the modification of the modal participation factor, in order to incorporate the effects of multi-support excitation into coherent response calculations. Also, the work by Michaltsos and Raftoyiannis must be quoted [3], which offered a theoretical approach for dealing with the aforementioned problems in bridges, subjected to near-source or long-distance earthquake motions. They developed a simple mathematical model for studying the phenomena as well as the conditions under which these may occur, while relevant safety indicators were derived.

(a)   (b)

Figure 1. Damaged Bridges: (a) Support damage of the Copper River bridge due to rocking, Alaska 1964 (from USGS Earthquake Hazards Program), and (b) Overturning of three spans of the Agua Caliente Bridge, Guatemala, 1976 (from Public Roads 40(3), pp.101-107, by J.D. Cooper) - reproduced from reference [3]

The modeling of overturning collapse and safety assessment of bridges supported on single-column piers, under multi-load patterns was investigated by Xiong et al. [4], applying 3D simulations (including superstructures, bearings, and pylons) and accounting for geometric and material nonlinearities. It was concluded that the specification-based methods greatly overrate the safety level, whereas the safety indicator provides more reasonable results up to the final collapse. Additionally, the anti-overturning stability of curved bridges under seismic action was studied by Deng et al. [5], and the effect on various parameters was evaluated.

The characteristics of extreme flood events (for example, the hurricane Ivan in the Gulf of Mexico [6]) and their impact on coastal bridges and other structures were and continue to be the subject of numerous publications and studies. Kosa [7] performed a damage analysis of bridges affected by the tsunami in the Great East Japan (Tohocu) Earthquake of March 11, 2011. The outflow conditions of 37 bridges were evaluated using the ratio of resistance to the tsunami force β. Two analytical approaches (video and numerical analyses) were conducted to evaluate the tsunami characteristics and outflow mechanisms of the girders. For each bridge, useful conclusions were drawn, regarding the tsunami action parameters. Furthermore, Yim et al. [8] developed an analytical plan for better understanding the tsunami loads on

structures, which include immediate, specific deterministic analysis, and experiments required to calculate the tsunami inundation models for the built environment as well as a comprehensive probability-based tsunami load estimation procedure. Azadbakht and Yim [9] examined the estimated tsunami loads of five California coastal bridges. The quantities of interest in their investigation were the horizontal forces, the vertical ones, and the overturning moments. Their simulation and analysis were conducted in two stages: (1) initial and overtopping, (2) full inundation, and a design procedure was proposed to compute the maximum forces on bridge superstructures. Good agreement between numerical predictions and formula estimations of the tsunami forces was observed.

Of great relevance to the content of the foregoing paper is the work by Xiang et al. [10]. There, representing a tsunami by a solitary wave, and through both large-scale experiments and numerical simulations, fluid impact forces on a representative coastal bridge deck (in the horizontal and vertical directions) due to inundation were investigated. A numerical parametric study (for determining the effects of bridge elevation variation and the wave height leads to an efficient and improved simplified procedure.

More experimental results combined with numerical simulations were reported in the work by Riggs et al. [11]. These are supplemented by the experimental results of Araki and Deguchi [12] on the bridge across the Narrow River, concerning tsunami fluid forces. The horizontal and vertical components of the tsunami fluid force acting on a bridge beam were measured through hydraulic experiments. The wave pressure on the bridge beam was also measured. The authors showed that the vertical component of the tsunami fluid force is as large as the horizontal component of the tsunami fluid force in several cases and that the wave pressure on a bridge beam is larger in the cases where the crest of larger incident waves hits the bridge. Noticeable is also the experimental study of tsunami-induced scour around a monopole foundation by Larsen et al. [13].

Of great interest is the research by Istrati et al. [14], in which deciphering the tsunami wave impact and associated connection forces in open-girder coastal bridges were reported and discussed. The paper was associated with the analysis of large-scale hydrodynamic experiments of tsunami wave impact on a bridge with open girders conducted in the Large Wave Flume at Oregon State University, based on the damage to coastal bridges during the tsunami in the Indian Ocean in 2004 and Japan in 2011. This analysis revealed that:

(a) tsunami bores introduce significant slamming forces, both horizontal (F_h) and uplift (F_v), during impact on the offshore girder and overhang; these can govern the uplift demand in connections,

(b) $maxF_h$ and $maxF_v$ do not always occur at the same time and contrary to the recommended practice, the simultaneous application of them at the center of gravity of the deck does not yield conservative estimates of the uplift demand in individual connections,

(c) the offshore connections must withstand the largest percentage of the total induced deck uplift among all connections,

(e) the generation of a significant overturning moment (OTM) at the initial impact when the slamming forces are maximized, which is the main reason for the increased uplift in the offshore connections, and

(f) neither $maxF_v$ nor $maxOTM$ always coincide with the maximum demand in each connection, suggesting the need to consider multiple combinations of forces with corresponding moments or with corresponding locations of application in order to identify the governing scenario for each structural component.

The findings suggested the need for a paradigm shift in the assessment of tsunami risk to coastal bridges to include not just the estimation of the total tsunami load on a bridge but also the distribution of this load to individual structural components necessary for the survival of the bridge.

Synolakis [15] showed that linear theory suffices for estimating the maximum runup height on plane beaches, while a very good review of this runup was also published [16]. The contents of these last two citations may be considered marginal, but provide a better overall insight.

Since a wide gap has separated studies by engineers and geologists on the characteristics of earthquakes and tsunamis, a symposium entitled "Frontiers of Earthquake/Tsunami Sedimentology and Disaster Mitigation" was organized at the Annual Meeting of the Geological Society of Japan (2008). Six very interesting papers were presented, bridging this gap [17]. Five years later (2013), Bricker and Nakayama published a case study [18] that dealt with the contribution of trapped air, deck superelevation, and nearby structures to bridge deck failure during a tsunami. Their work, based on two models, showed that factors contributing to failure included the presence of seawall near the bridge, an inclination of the deck upward toward the ocean, sediment entrained in the water, and the air trapped between girders.

Greco, Lonetti and Nevone Blasi [19] conducted vulnerability analyses of bridge structures acted upon by extreme flood or tsunami loads, in view of loading variability and structural and fluid characteristics. Using a sophisticated numerical model based on phase field theory and 3D solid simulation, the authors quantified the Dynamic Amplification Effects (DAEs) produced by external loads with respect to conventional static analyses and discussed the influences of bridge deformations on the hydrodynamic loads and vice versa.

The same investigators [20] in a similar perspective quantified the aforementioned DAEs on the basis of the formulations proposed by existing codes and discussed protection and mitigation measures.

There are also several verification studies by FEM and other numerical approaches dealing with fluid-structure interaction problems [21]-[26]. Finally, one may refer to an investigation dealing with the behavior of specific bridges [27]-[32].

The current codes [33]-[35] offer, a description of the tsunami phenomenon, some instructions, and in some cases diagrams of the developed waves and their intensity in relation to the depth and slope of the sea bottom.

In May 2021, the Pacific Earthquake Engineering Research Center (PEER) released the "Tsunami Design Guidelines for New Bridges", based on reports FHWA-OR-RD-21-12 [36] and FHWA-OR-RD-21-13 [37] by D. Istrati and I.G. Buckle.

As the long bridges (suspension or cable-stayed ones) due to navigation reasons have a deck built quite high above the sea level, this paper deals with short- or medium-sized bridges having a height above the sea level that allows the action of tsunami waves.

Based on the scarcity and excessive complexity of existing models, as described above, in this work, a simplified continuum approach is proposed, in order to establish extreme flood actions (acting wave and impact ones) on superstructures of bridges. This approach, based on relations stemming from the principles of hydraulics, allows for the determination of horizontal and vertical forces, as well as of drag forces and overturning moments. In special cases, one should also consider buoyancy forces, which can often have a particular influence.

Namely, in Section 5, we suppose that the reactions of the bearings are satisfactory. Thus, the bridge remains in place deformed by the external dynamic actions. Contrarily, in Section 6, we assume that the bearings are incapable of withstanding the acting forces. Thus, we study the safety of the bridge against rocking, shifting, and overturning phenomena, taking into account the realistic bearing conditions of the deck. It would also be useful to provide some basic information about the generation and propagation of tsunami waves. Two kinds of bridges have been studied. The high bridge is affected by impact forces only and the relatively low bridge where, in addition, buoyancy forces also act.

Finally, in Section 8, a comparison between the results obtained here and the ones from FE and other numerical approaches is performed, leading to the conclusion that the former is of acceptable accuracy for practice and has minimal computational and time costs, as compared to other sophisticated simulations. Section 9 summarizes the main findings of this work.

2. The tsunamis

The sinking or lifting of a suddenly activated fault at the sea bed causes the water to recede or swell. In both cases, the produced disturbance causes the birth of a small, medium, or very strong tsunami, whose energy is transmitted throughout the water column regardless of the ocean's depth. A series of very long waves travel outward on the surface of the ocean. Their wavelengths and periods depend on the dimensions of the event source and vary with the depth of the water according to Figure 2. As the waves approach the coast, the wavelength decreases, and their height increases. Finally, the wave velocity depends on the water depth according to Eq.1 of [38], which satisfactorily estimates the magnitude of the velocity.

$$v_0(h) = \sqrt{g \cdot h_s} \ \left(\text{in m/s}\right) \ \text{for } h_s < 0.05 \text{ of wavelength} \tag{1}$$

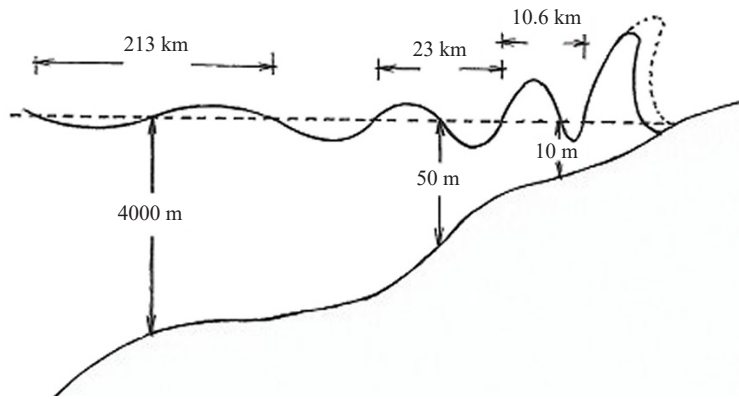The changes in wavelength and wave velocity are shown in Figure 3.

Figure 2. Wavelengths in relation to water depth (from National Geographic, slightly retouched)
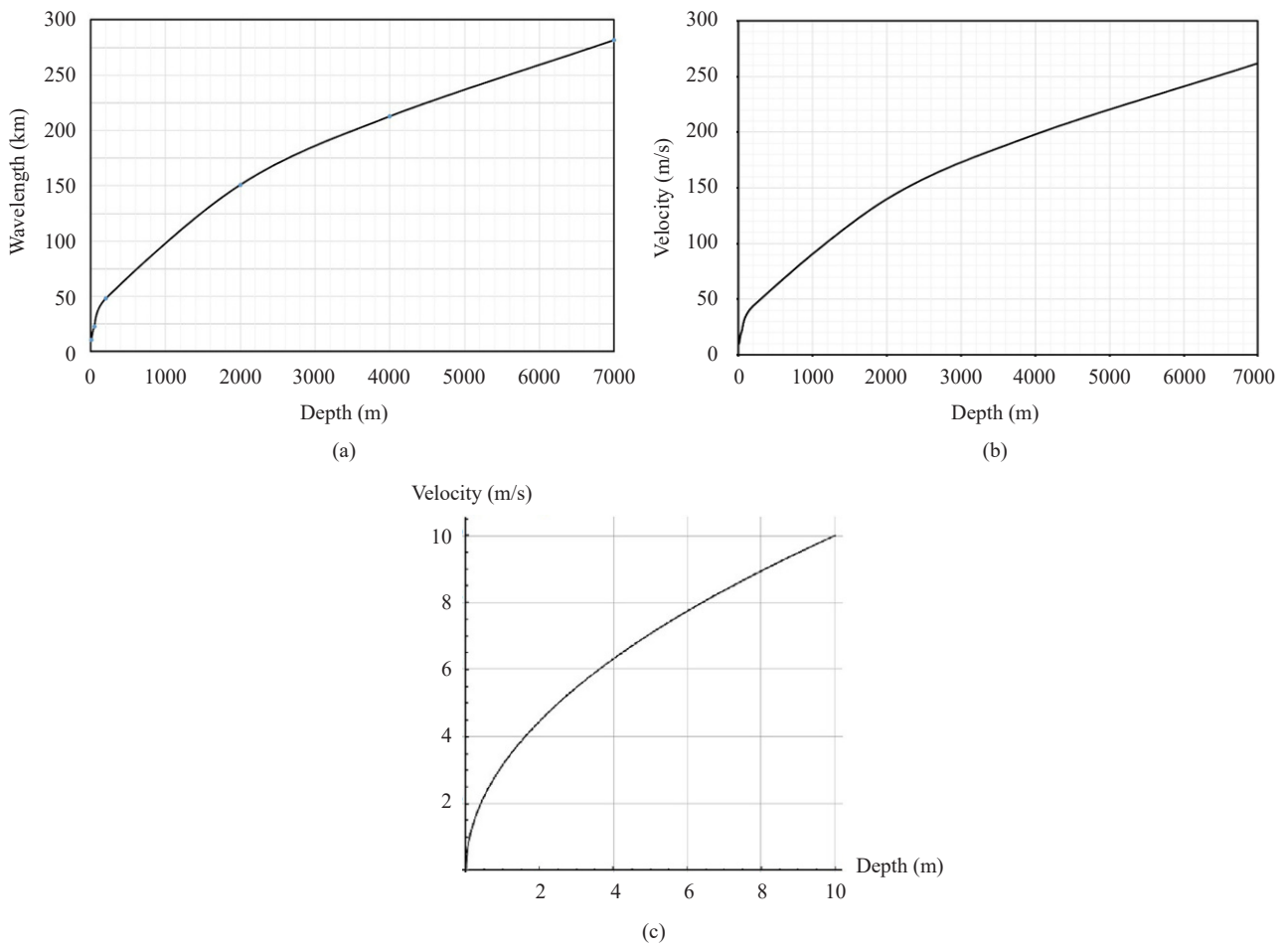

Figure 3. (a) Wavelength vs seawater depth, (b) velocity vs seawater depth, and (c) velocity vs small seawater depth

The above graphs are based on the contents of Table 1, where some characteristic values for a strong tsunami can be found.

Table 1. Characteristic values of measured/observed tsunamis' properties

Depth (m)	Velocity (km/h)	Wavelength (km)
7,000	943	282
4,000	713	213
2,000	504	151
200	159	48
50	79	23
10	36	10.6

The height of waves impacting the coast does not obey the laws of classical wave engineering. For example, the tsunami in the Indian Ocean (2004) gave waves 30 m in height in Indonesia, 13 m in Sri Lanka, and 10 m in Somalia. In any case, the highest recorded waves were in Krakatoa (1893), h = 40 m, and Japan (2011), h = 41 m.

For the study of coastal waves, many theories have been developed so far. The most known are the 2nd and 3rd-degree theory of Stokes, the Gerstner theory, the Cnoidal theory, and the theory of Solitary Waves. The latter is of particular interest since it significantly approaches tsunami waves. In this theory, each wave is studied separately. The wave propagates on the free surface of the sea like a bulge without the presence of an abdomen. The water molecules are motionless and as soon as the wave passes over them, they move forward, following an arc path if they are on the surface, and a straight path when they are at the bottom of the sea.

The following relation gives the velocity of the solitary wave:

$$v_o = \sqrt{g \cdot (h + h_s)} \tag{2}$$

In practice, these waves are to be considered solitary ones, appearing in very shallow waters, while their peaks are larger than distance s (Figure 4), where

$$s \geq 2 \cdot \pi \cdot h_s \cdot \sqrt{\frac{h_s}{3 \cdot h}} \tag{3}$$
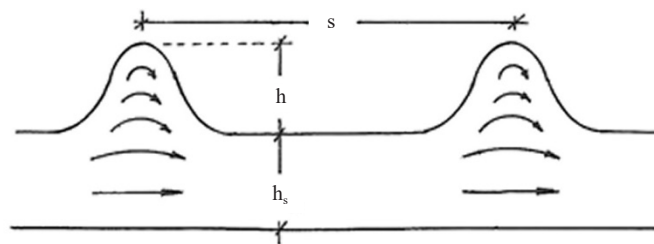
Figure 4. Solitary waves

In Figure 5, the comparison of Eqs. (1) and (2), for different values of depth, h_s is illustrated, from which it is observed that for $h_s > 30$ m, the formulae practically converge.
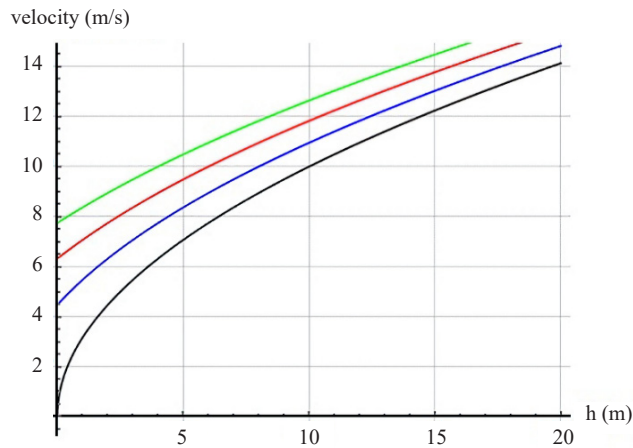
Figure 5. Comparison of relation (1)-black curve and (2), for $h_s = 2$ m (blue), $h_s = 4$ m (red), and $h_s = 6$ m (green)

3. Loads and loading models

3.1 *The geometry of the wave*

Let us now consider the random wave in Figure 6, approaching the coast and caused by a tsunami. For easier mathematical processing, we reshape the form of the wave as close as possible to its real one, as shown by a dashed line in the aforementioned Figure.
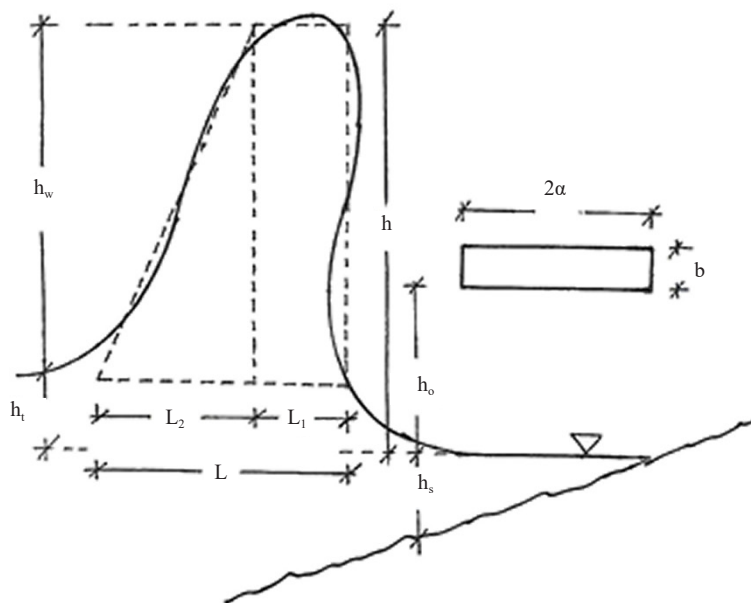

Figure 6. The geometry of the wave

From observations and laboratory results [11-14], the main dimensions of the oncoming wave are its height h, its width L, and the height of the sea level rise h_t.

It has also been observed that L varies from 0.5 h to h, h_t from zero to 0.4 h, and L_2 from L_1 to 1.5 L_1. The most critical factor is the velocity v_o of the wave approaching the bridge, which is given as a function of depth h_s by Eqs. (1) or (2). Finally, no one can prescribe the ratio h/L.

3.2 The possible loading models - scenarios

There is a critical height h_{cr} of the oncoming wave. For $h > h_{cr}$, the wave falls on the entire deck of the bridge; otherwise, it falls on a part of the deck. Setting $s = 2\alpha$ in the contents of Appendix A3, we determine $h_{eff} = \dfrac{2 \cdot g \cdot \alpha^2}{v_o^2}$ and finally one may write that

$$h_{cr} = h_o + b + \frac{2 \cdot g \cdot \alpha^2}{v_o^2} \tag{4}$$

The critical height of a wave, required for it to land on the entire deck, is determined by inserting v_o from Eq. (2) into Eq. (4). This leads to $h_r = h_o + b + \dfrac{2 \cdot g \cdot \alpha^2}{g \cdot (h_{cr} + h_s)}$, and hence, the following algebraic equation is reached: $h_{cr}^2 + (h_s - h_o - b) \cdot h_s - 2 \cdot \alpha^2 = 0$; its solution is given by

$$h_{cr} = \frac{(h_o + b - h_s) + \sqrt{(h_o + b - h_s)^2 + 4 \cdot [(h_o + b) \cdot h_s + 2 \cdot \alpha^2]}}{2} \tag{5}$$

There are several possible models - scenarios for tsunami impact, on which the acting forces depend. The most characteristic ones, according to the authors' opinion, are the four shown in Figure 7.

If $h \leq h_s + h_o + b$, scenario (a) occurs; if $h_s + h_o + b \leq h \leq h_{cr}$, scenario (b) occurs; if $h_{cr} \leq h$, then scenario (c) occurs; and finally, when relations $h_t = h_o$ and $t_{ar} > (L_1 + L_2)/v_o$ are valid (where t_{ar} is the time required for the arrival of the second wave, which usually has a height smaller than h/2), scenario (d) is in order.
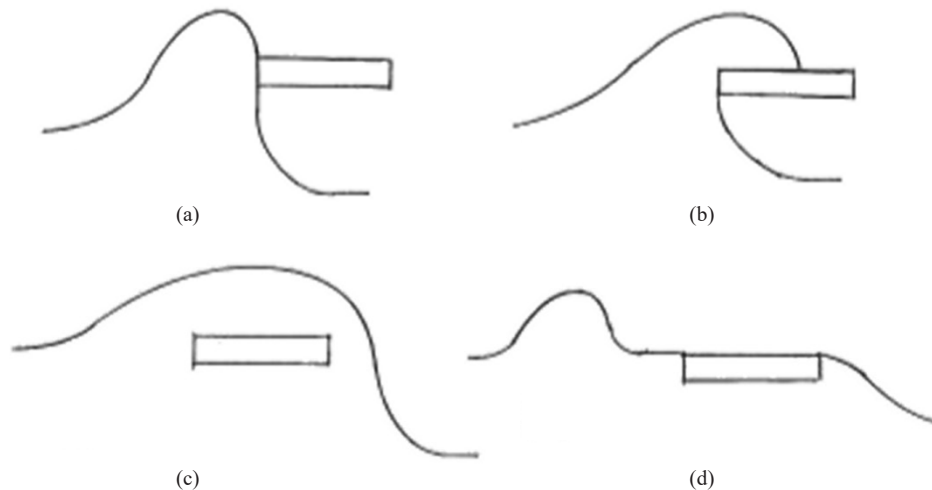

(a)　　　　(b)

(c)　　　　(d)

Figure 7. The possible models/scenarios

3.3 The acting generalized forces

We assume that the water falling on the deck produces only impact forces and then recedes. We divide the lengths L_1 and L_2 of the wave into n_1 and n_2 water columns, respectively, as shown in Figure 8a, while

$$n_1, n_2 \to \infty \tag{6}$$

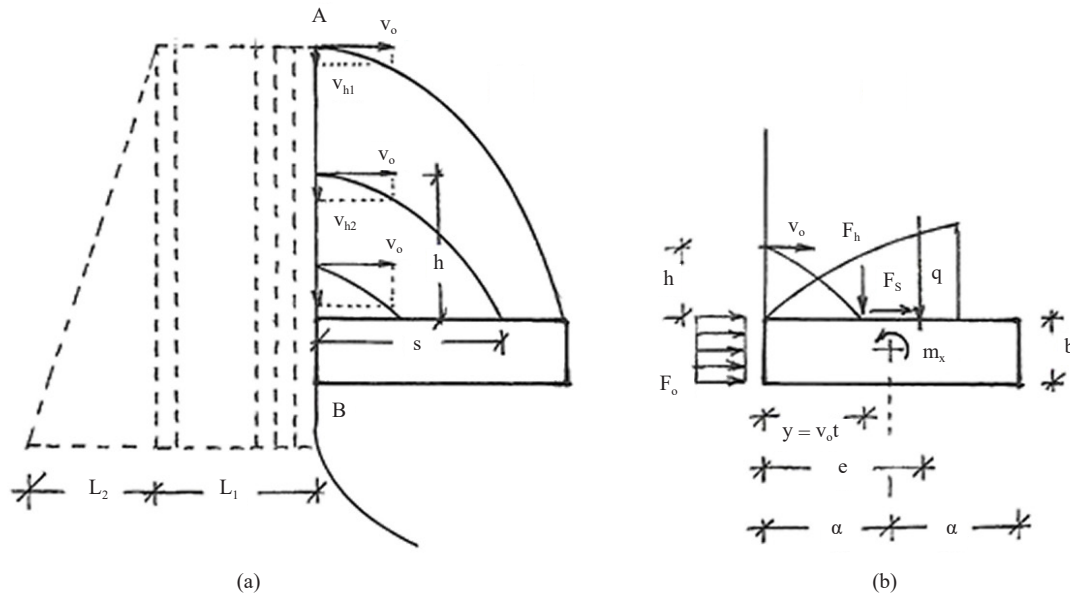**Figure 8.** The water columns (a) and the forces acting on the deck (b)

When the ith infinitesimal water column L_1/n_1 of the critical wave reaches the bridge, the water of the front AB starts falling on the deck at times $t_i = (i-1)L_1/n_1 v_o$ with the same initial horizontal velocity v_o, but at different time instances, depending on the height h. For a loading model-scenario such as the one in Figure 7b, the applied forces on a deck of dimensions $2a \cdot b$ due to a random water column are illustrated in Figure 8b.

According to the contents of Appendices A2 and A3, the applied distributed forces F_w, F_s, and F_o caused by the water volume unit $f_1 = dV = \dfrac{L_1}{n_1} \cdot 1 \cdot 1$ are:

$$F_w = \frac{\gamma}{g} \cdot f_1 \cdot v^2 \cdot sin\varphi \tag{7}$$

$$F_s = \frac{\gamma}{g} \cdot f_1 \cdot v^2 \cdot cos\varphi \tag{8}$$

$$F_o = \frac{\gamma}{g} \cdot f_1 \cdot v_o^2 \tag{9}$$

For the random water vein of Figure A3 $sin\varphi = v_h/v$ and $cos\varphi = v_o/v$ and therefore, expressions (7-9) take the following form:

$$F_w = \frac{\gamma}{g} \cdot f_1 \cdot v_h \cdot v \tag{10}$$

$$F_s = \frac{\gamma}{g} \cdot f_1 \cdot v_o \cdot v \tag{11}$$

$$F_o = \frac{\gamma}{g} \cdot f_1 \cdot v_o^2 \tag{12}$$

where

$$v_o = constant \tag{13}$$

$$v_h = g \cdot t \tag{14}$$

$$v = \sqrt{v_o^2 + g^2 \cdot t^2} \tag{15}$$

4. The loadings

The loadings due to the falling water up to time t, corresponding to the acting forces given above, are as follows:

4.1 *Vertical loading*

$$q_{z1}(x,t) = \frac{L_1}{n_1} \cdot \int_0^t F_w dt, \ 0 \le t \le \frac{L_1}{v_o} \tag{16}$$

$$q_{z2}(x,t) = \frac{L_2}{n_2} \cdot \int_0^t F_w dt, \ \frac{L_1}{v_o} \le t \le \frac{L_1 + L_2}{v_o} \tag{17}$$

4.2 *Lateral loading*

$$q_{y1}(x,t) = -\frac{L_1}{n_1} \cdot \int_0^t F_s dt - b \cdot F_o, \ 0 \le t \le \frac{L_1}{v_o} \tag{18}$$

$$q_{y2}(x,t) = -\frac{L_2}{n_2} \cdot \int_0^t F_s dt - b \cdot F_o, \ \frac{L_1}{v_o} \le t \le \frac{L_1 + L_2}{v_o} \tag{19}$$

4.3 *Torsional loading*

$$m_{x1}(x,t) = \frac{L_1}{n_1} \cdot \left(\int_0^t (\alpha - v_o \cdot t) \cdot F_w dt - \frac{b}{2} \cdot \int_0^t F_s dt \right), \ 0 \le t \le \frac{L_1}{v_o} \tag{20}$$

$$m_{x2}(x,t) = \frac{L_2}{n_2} \cdot \left(\int_0^t (\alpha - v_o \cdot t) \cdot F_w dt - \frac{b}{2} \cdot \int_0^t F_s dt \right), \ \frac{L_1}{v_o} \le t \le \frac{L_1 + L_2}{v_o} \tag{21}$$

5. The motion of the bridge
5.1 *Governing equations*

The following relations give the equations governing the dynamic behavior of a single-span bridge, as the one in

Figure 9a:

$$EI_y w'''' + c\dot{w} + m\ddot{w} = Q_z(x,t) = Q_z(x) \cdot f_z(t) \tag{22}$$

$$EI_z \upsilon'''' - EI_z z_M \theta'''' - GI_D \theta'' + c\dot{\upsilon} + m\ddot{\upsilon} = Q_y(x,t) = Q_y(x) \cdot f_y(t) \tag{23}$$

$$EI_\omega \theta'''' - EI_z z_M \upsilon'''' - GI_D \theta'' + c\dot{\theta} + I_{px}\ddot{\theta} = M_x(x,t) = M_x(x) \cdot f_x(t) \tag{24}$$

where EI_y, EI_z, GI_D, and EI_ω are the bending, the torsional, and the warping rigidities of the bridge cross-section respectively, m is the mass per unit length, and I_{px} is the rotational inertia of the bridge, c is the damping coefficient, z_M is the distance between the center of gravity and the shear center, and Q_y, Q_z, and M_x are the external loads.

Noting that Eq. (22) is independent of the remaining two, we are seeking a solution of the form

$$w(x,t) = \sum_n W_n(x) \cdot P_n(t) \tag{25}$$

$$\upsilon(x,t) = \sum_n V_n(x) \cdot T_n(t) \tag{26}$$

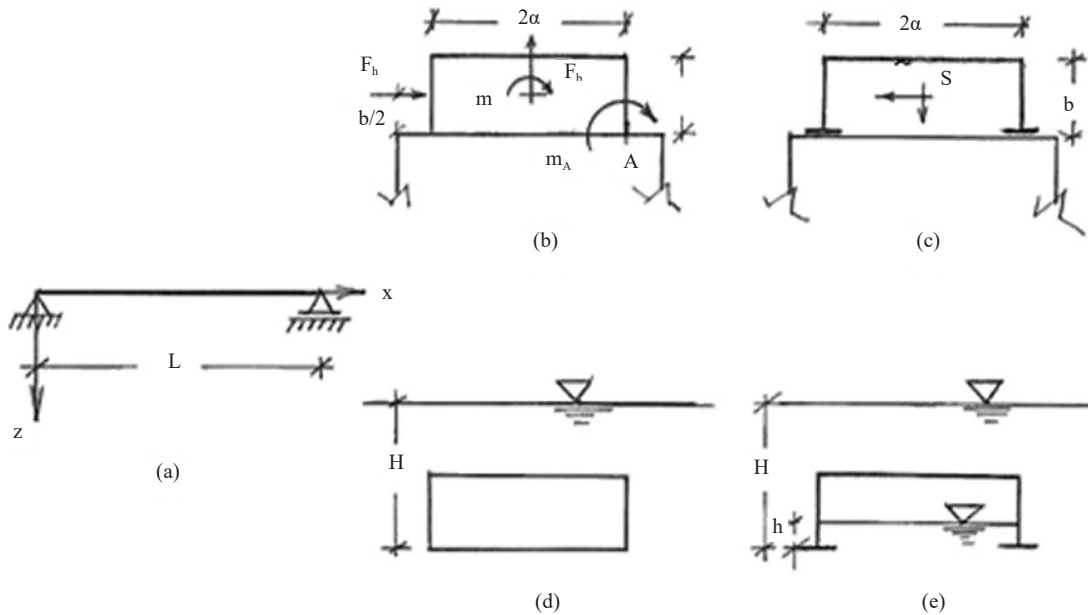$$\theta(x,t) = \sum_n \Phi_n(x) \cdot T_n(t) \tag{27}$$

Figure 9. (a) Single-span bridge, (b) closed cross-section, (c) open cross-section, (d), (e) buoyancy forces

When $z_M = 0$, Eqs. (23) and (24) become independent of each other and can be easily solved as Eq. (22).

5.2 Vertical motion
5.2.1 $0 \le t \le \dfrac{L_1}{v_o}$

The equation of vertical motion of a simple-span bridge, as shown in Figure 10a, is given by Eq. (22). We are

searching for a solution in the form of Eq. (25). Following a well-known procedure of linearized dynamics, we obtain the formula (28), for the time function:

$$P_{1n}(t) = \frac{\int_0^L \frac{\gamma}{g} \cdot \frac{L_1}{n_1} \cdot W_n dx}{\bar{\omega}_{zn} m \int_0^L W_n^2 dx} \int_0^t \left(\int_0^\tau v_h(\tau) v(\tau) d\tau \right) \cdot e^{-\beta \cdot (t-\tau)} \cdot sin[\bar{\omega}_{zn}(t-\tau)] d\tau \qquad (28)$$

for

$$\frac{(i-1) \cdot L_1}{n_1 \cdot v_o} \le t \le \frac{(i-1) \cdot L_1}{n_1 \cdot v_o} + \sqrt{\frac{2 \cdot h}{g}} = t_{bi} \qquad (29)$$

where

$$\bar{\omega}_{zn} = \sqrt{\omega_{zn}^2 - \beta^2} \qquad (30)$$

For $t > t_{bi}$, the bridge vibrates freely, and its dynamic flexural deflection is

$$w_f = \sum_n W_{n(x)} \cdot P_{f1n}(t) \qquad (31)$$

$$P_{f1n}(t) = e^{-\beta \cdot (t-t_{bi})} \cdot \left(A_n sin[\omega_{zn}(t-t_{bi})] + B_n sin[\omega_{zn}(t-t_{bi})] \right) \qquad (32)$$

Using the initial conditions $P_{1n}(t_{bi}) = P_{f1n}(t_{bi})$ and $\dot{P}_{1n}(t_{bi}) = \dot{P}_{f1n}(t_{bi})$, we determine the expressions of constants A_n and B_n, given by

$$A_n = -\frac{\beta \cdot P_{1n}(t_{bi}) + \dot{P}_{1n}(t_{bi})}{\omega_{zn}}, \ B_n = P_{1n}(t_{bi}) \qquad (33)$$

The total produced vertical deformation due to the wave part L_1 yields:

$$w_1(x,t) = \sum_{i=0}^{n_1-1} \left(\sum_n W_n(x) P_{1n}(t) \cdot \left\{ \begin{array}{c} H\left[t - \frac{i \cdot L_1}{n_1 \cdot v_o} \right] \\ -H\left[t - \frac{i \cdot L_1}{n_1 \cdot v_o} - \sqrt{\frac{2 \cdot h}{g}} \right] \end{array} \right\} \right)$$

$$+ \sum_{i=0}^{n_1-1} \left(\sum_n W_n(x) P_{f1n}(t) \cdot H\left[t - \frac{(i-1) \cdot L_1}{n_1 \cdot v_o} - \sqrt{\frac{2 \cdot h}{g}} \right] \right) \qquad (34)$$

5.2.2 $t > \dfrac{L_1}{v_o}$

Via a similar procedure, as the one described above, we determine that

$$P_{2n}(t) = \frac{\int_0^L \frac{\gamma}{g} \cdot \frac{L_2}{n_2} \cdot W_n dx}{\overline{\omega}_{zn} m \int_0^L W_n^2 dx} \cdot \int_0^t \left(\int_0^\tau v_h(\tau)v(\tau)d\tau \right) \cdot e^{-\beta \cdot (t-\tau)} \cdot sin[\overline{\omega}_{zn}(t-\tau)]d\tau \tag{35}$$

$$t_{bj} = \frac{(j-1) \cdot L_2}{n_2 \cdot v_o} + \frac{L_1}{v_o} + \sqrt{\frac{2 \cdot h}{g} \cdot \frac{n_2 - j}{n_2}} \tag{36}$$

$$P_{f2n}(t) = e^{-\beta \cdot (t-t_{bj})} \cdot \left(A_n sin[\omega_{zn}(t-t_{bj})] + B_n sin[\omega_{zn}(t-t_{bj})] \right) \tag{37}$$

$$A_{nf} = -\frac{\beta \cdot T_{2n}(t_{bj}) + \dot{T}_{2n}(t_{bj})}{\omega_{zn}}, \; B_{fn} = T_{2n}(t_{bj}) \tag{38}$$

$$w_2(x,t) = \sum_{j=0}^{n_2-1} \left(\sum_n W_n(x)P_{2n}(t) \cdot \left\{ \begin{array}{c} H\left[t - \dfrac{j \cdot L_2}{n_2 \cdot v_o} - \dfrac{L_1}{v_o} \right] \\ -H\left[t - \dfrac{j \cdot L_2}{n_2 \cdot v_o} - \dfrac{L_1}{v_o} - \sqrt{\dfrac{2 \cdot h}{g} \cdot \dfrac{n_2 - j}{n_2}} \right] \end{array} \right\} \right)$$

$$+ \sum_{j=0}^{n_2-1} \left(\sum_n W_n(x)P_{f2n}(t) \cdot H\left[t - \frac{(j-1) \cdot L_2}{n_2 \cdot v_o} - \frac{L_1}{v_o} - \sqrt{\frac{2 \cdot h}{g} \cdot \frac{n_2 - j}{n_2}} \right] \right) \tag{39}$$

5.3 *Lateral motion*

We assume, without loss of generality, that $z_M = 0$. Thus, Eqs. (26) and (27) become uncoupled, and therefore, we are searching for a solution to the form:

$$\upsilon(x,t) = \sum_n V_n(x) \cdot T_n(t) \tag{40}$$

The acting forces F_s and F_o are given by expressions (11) and (12), while the corresponding loadings are equal to:

$$q_{y1} = q_{y1a} + q_{yb} \tag{41}$$

$$q_{y2} = q_{y2a} + q_{yb} \tag{42}$$

where

$$q_{y1a}(x,t) = -\frac{L_1}{n_1} \int_0^t F_s dt, \; 0 \le t \le \frac{L_1}{v_o} \tag{43}$$

$$q_{y2a}(x,t) = -\frac{L_2}{n_2} \int_0^t F_s dt, \; \frac{L_1}{v_o} \le t \le \frac{L_1 + L_2}{v_o} \tag{44}$$

$$q_{yb} = -b \cdot F_o \tag{45}$$

Deformation $v_1(x, t)$, due to the loading of (43) and (44), is given by the expressions of §5.2.1 and §5.2.2, where V and T are placed instead of W and P, respectively, and ω_{yn} instead of ω_{zn}.

Deformation $v_2(x, t)$, due to loading of (45) is given by the following relations:

$$\upsilon_2(x,t) = \sum_n V_n \cdot G_n \cdot \left[H(t-0) - H\left(t - \frac{L_1 + L_2}{v_o}\right) \right], \ 0 \le t \le t_o \tag{46}$$

$$\upsilon_{2f}(x,t) = \sum_n V_n \cdot G_{nf} \cdot H\left(t - \frac{L_1 + L_2}{v_o}\right), \ t > t_o \tag{47}$$

where V_n are the shape functions, while

$$G_n = \int_0^t q_{y2}(x,\tau) \cdot e^{-\beta \cdot (t-\tau)} \cdot \sin\omega_{yn}(t-\tau) d\tau \tag{48}$$

$$G_{nf} = e^{-\beta \cdot (t-t_o)} \cdot C_n \cdot \sin\omega_{yn}(t-t_o) + D_n \cdot \cos\omega_{yn}(t-t_o) \tag{49}$$

$$C_n = -\frac{\beta \cdot G_n(t_o) + \dot{G}_n(t_o)}{\omega_{yn}} \tag{50}$$

$$D_n = G_n(t_o) \tag{51}$$

$$t_o = \frac{L_1 + L_2}{v_o} \tag{52}$$

5.4 *Torsional motion*

The acting forces F_w and F_s are given by expressions (10) and (11), while the corresponding loadings are equal to

$$m_{x1}(x,t) = \int_0^t (\alpha - v_o \cdot t) \cdot F_w dt \tag{53}$$

$$m_{x2}(x,t) = -\frac{b}{2} \cdot \int_0^t F_s dt \tag{54}$$

Again, we are seeking a solution of the form

$$\theta(x,t) = \sum_n \Phi_n(x) \cdot R_n(t) \tag{55}$$

Deformation $\theta_1(x, t)$, due to loading (53), is given by the expressions of §5.2.1 and §5.2.2, where Φ and R are placed instead of W and P, respectively, and $\omega_{\theta n}$ instead of ω_{zn}.

Deformation $\theta_2(x, t)$, due to loading (54), is given by the following relations, where Φ_n are the related shape functions:

$$\theta_2(x,t) = \sum_n \Phi_n \cdot K_n \cdot \left[H(t-0) - H\left(t - \frac{L_1 + L_2}{v_o}\right) \right], \ 0 \le t \le t_o \tag{56}$$

$$\theta_{2f}(x,t) = \sum_n \Phi_n \cdot K_{nf} \cdot H\left(t - \frac{L_1 + L_2}{v_o}\right), \ t > t_o \tag{57}$$

while

$$K_n = \int_0^t m_{x2}(x,\tau) \cdot e^{-\beta \cdot (t-\tau)} \cdot sin\omega_{\theta n}(t-\tau)]d\tau \tag{58}$$

$$K_{nf} = e^{-\beta \cdot (t-t_o)} \cdot C_n \cdot sin\omega_{\theta n}(t-t_o) + D_n \cdot cos\omega_{\theta n}(t-t_o) \tag{59}$$

$$C_n = -\frac{\beta \cdot K_n(t_o) + \dot{K}_n(t_o)}{\omega_{\theta n}} \tag{60}$$

$$D_n = K_n(t_o) \tag{61}$$

$$t_o = \frac{L_1 + L_2}{v_o} \tag{62}$$

6. Bridge safety

In the previous section, the motion and deformations of the bridge deck were studied, provided that it is adequately anchored to the pylons or the bearings of the bridge. However, these conditions are not always met. In this section, we will study the safety of a bridge under the action of a tsunami, accounting for rocking, shifting, and overturning phenomena and the realistic bearing conditions of the deck.

6.1 *Acting generalized forces*

The generalized forces causing the aforementioned phenomena are the ones shown in Figure 9b.

6.1.1 *Buoyancy forces F_b*

For a closed cross-section, these are equal to:

$$F_b = 2 \cdot \alpha \cdot b \cdot \gamma \cdot L \tag{63}$$

while for an open cross-section, if the water can escape, buoyancy forces do not appear. When the water has no way to escape, then the bridge behaves as a diving bell; this is shown in Figure 9e.

We consider that before the tsunami, the bridge is under atmospheric pressure p_o, while the volume of the bridge part that will act as a diving bell is $V_o = 2\alpha \frac{b}{2} = \alpha b$. Additionally, we assume that the bridge is covered by water to a height equal to H, while the water rises inside the bridge to a height h (see Figure 9e). Therefore, the pressure inside the bell will be $p = p_o + (H-h) \cdot \gamma$ (with γ the specific weight of the water). The volume of the trapped air will be $V = 2\alpha\left(\frac{b}{2} - h\right)$.

According to the law of Boyle-Marriot, we obtain $p_o V_o = pV$ or $p_o \cdot \alpha \cdot b = [p_o + (H - h) \cdot \gamma] \cdot 2\alpha \cdot \left(\dfrac{b}{2} - h \right)$, leading to

the equation: $h^2 - \left(\dfrac{p_o}{\gamma} + \dfrac{b}{2} + H \right) \cdot h + \dfrac{H \cdot b}{2} = 0$, which possesses the following solution:

$$h = \frac{\left(\dfrac{p_o}{\gamma} + \dfrac{b}{2} + H \right) - \sqrt{\left(\dfrac{p_o}{\gamma} + \dfrac{b}{2} + H \right)^2 - 2Hb}}{2} \tag{64}$$

Hence, the buoyancy forces are given by:

$$F_b = 2 \cdot \alpha \cdot \left(\frac{b}{2} - h \right) \cdot \gamma \cdot L \tag{65}$$

6.1.2 Forces F_h

These, due to models-scenarios (a) or (b) of Figure 8, are equal to:

$$F_h = \frac{\gamma}{g} \cdot b \cdot L \cdot v_o^2 \tag{66}$$

6.1.3 Moment m_b

Finally, moment m_b, acting about the right bearings of the bridge is:

$$m_b = \left(\frac{L_1}{n_1} \cdot \int_0^{\frac{L_1}{v_o}} (a - v_o \cdot t) \cdot F_w dt - b \cdot \int_0^{\frac{L_1}{v_o}} F_s dt - \frac{b}{2} \cdot F_b \right) \cdot L \tag{67}$$

6.2 Reacting forces

The generalized forces that react to those of catastrophe are depicted in Figure 10.
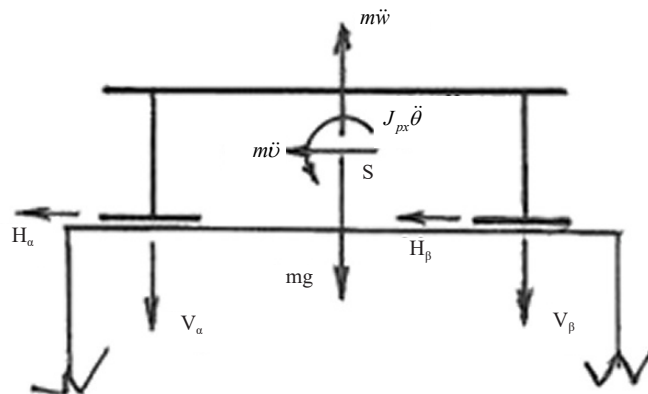
Figure 10. Reacting generalized forces

In particular, the reacting forces come from (a) the weight of the deck, (b) the bearings, (c) friction, and (d) inertia actions.

The weight of the deck is usually the main reacting force and is equal to:

$$F_{br} = m \cdot g \cdot L \tag{68}$$

The bearings in practice however are not equipped with elements capable of developing satisfactory lateral or torsional reacting forces. Assuming that each bearing has n bolts of diameter d, we will have:

$$\left. \begin{array}{l} \text{Tensile reaction: } F_{bt} = n \cdot \dfrac{\pi \cdot d^2}{4} \cdot \sigma_f \\[3mm] \text{Shear reaction: } F_{bs} = n \cdot \dfrac{\pi \cdot d^2}{4} \cdot \tau_f \end{array} \right\} \tag{69}$$

where σ_f and τ_f are the tensile and shear yield strengths, respectively.

Moreover, supposing that there is some connection between the bridge and pedestal, the friction forces can react to horizontal actions. If μ is the friction coefficient between steel elements ($\cong 0.015$), then

$$F_{bf} = \mu \cdot m \cdot g \cdot L \tag{70}$$

Finally, the inertia actions F_{bir}, F_{bis}, m_{bio} against rocking, shifting, and overturning, respectively, due to the sudden elastic deformation of the deck at time $\Delta t \to 0$, which can be obtained from Section 5.

6.3 *The rocking phenomenon*

This can only occur if

$$F_b - (F_{br} + F_{bt} + F_{bir}) \geq 0 \tag{71}$$

Inertia forces F_{bir} may develop or not, depending on the sudden or not appearance of the buoyancy forces. In the former case, these usually act simultaneously with shifting and overturning forces.

6.4 *The shifting phenomenon*

This occurs under the following condition:

$$F_h - (F_{bs} + F_{bf} + F_{bis}) \geq 0 \tag{72}$$

6.5 *The overturning phenomenon*

Assuming that the bridge will rotate about the axis of the right bearings, this phenomenon occurs when:

$$m_b - (2 \cdot \alpha \cdot F_{bt} + \alpha \cdot F_{br} + F_{bio}) \geq 0 \tag{73}$$

7. Numerical examples and discussion
7.1 *The bridge*

Let us consider two simply supported bridges with lengths $L = 16$ m, and $L = 70$ m, having a doubly symmetric

cross-section ($z_M = 0$) and dimensions $2\alpha \times b = 10 \times 1$ and $2\alpha \times b = 10 \times 3$.

Respectively, as depicted in Figure 11, they are made from structural steel (isotropic and homogeneous material) with a modulus of elasticity $E = 2.1 \times 10^8$ kN/m^2, and shear modulus $G = 0.8 \times 10^8$ kN/m^2.

The bridge of length 16 m has moments of inertia $I_y = 0.007$ m^4, $I_z = 0.08$ m^4, torsional constant $I_d = 0.2 \times 10^{-3}$ m^4, warping constant $I_w = 0.08$ m^6, mass per unit length $m = 300$ kg/m and rotational inertia $I_{px} = 500$ kgm^2. The one of 70 m has moments of inertia $I_y = 0.80$ m^4, $I_z = 8.50$ m^4, torsional constant $I_d = 0.50$ m^4, warping constant $I_w = 0.10$ m^6, mass per unit length $m = 800$ kg/m and rotational inertia $I_{px} = 2,500$ kgm^2.
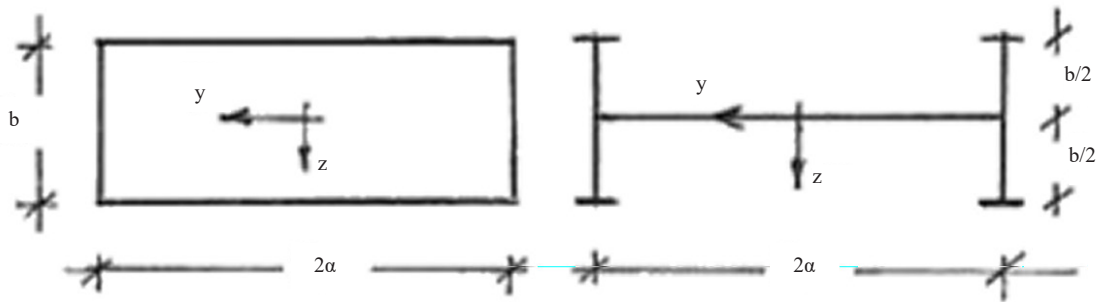
Figure 11. The cross-sectional geometry of a simply supported bridge

Thus, their calculated natural frequencies are:
a. Bridge of 16 m
For bending parallel to z-axis: $\omega_{z1} = 26.99$, $\omega_{z2} = 107.95$, $\omega_{z3} = 242.88$ (s^{-1})
For bending parallel to y-axis: $\omega_{y1} = 91.23$, $\omega_{z2} = 364.93$, $\omega_{z3} = 821.10$ (s^{-1})
For rotation about x-axis: $\omega_{\theta1} = 71.54$, $\omega_{\theta2} = 283.55$, $\omega_{\theta3} = 636.89$ (s^{-1})
b. Bridge of 70 m
For bending parallel to z-axis: $\omega_{z1} = 9.23$, $\omega_{z2} = 36.82$, $\omega_{z3} = 83.07$ (s^{-1})
For bending parallel to y-axis: $\omega_{y1} = 30.08$, $\omega_{z2} = 120.35$, $\omega_{z3} = 270.73$ (s^{-1})
For rotation about x-axis: $\omega_{\theta1} = 56.80$, $\omega_{\theta2} = 113.78$, $\omega_{\theta3} = 171.12$ (s^{-1})
For both cases, we consider that each bearing is usually anchored by two M20 Grade 5.8 bolts ($\sigma_f = 5,000$ dN/cm^2, $\tau_f = 4,000$ dN/cm^2).

7.2 The wave

In this section, we examine the influence of some parameters on the wave characteristics and the magnitude of loadings.

7.2.1 The influence of a

In the plots of Figure 12, we perceive the relationship between the critical height h and the half-width a of the deck for three values of the distance h_o of the deck from the water level. These elements strongly affect the critical height of the upcoming wave.

7.2.2 The change of v_0

In the curves of Figure 13, we observe the relationship between the velocity v_o of the upcoming wave and the height h of the wave for three values of the water depth h_s. The above parameters strongly affect the velocity of the upcoming wave.
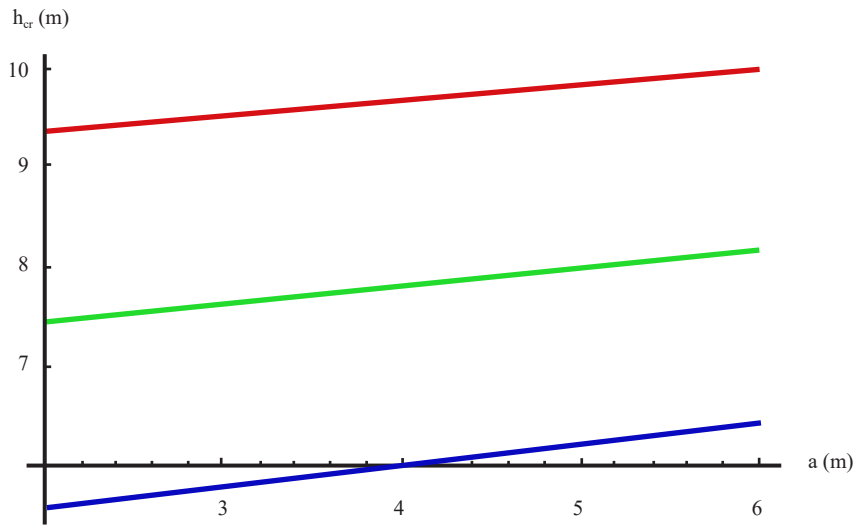
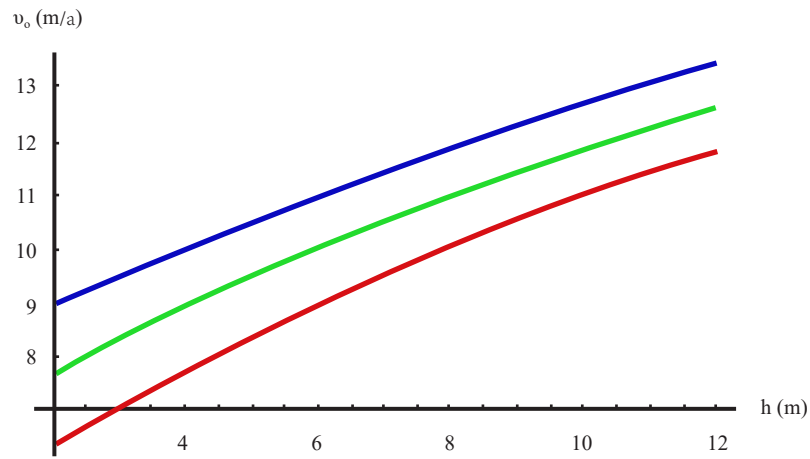**Figure 12.** The influence of α on h_{cr} for $h_o = 6$ m (red), 4 m (green), and 2 m (blue)

Figure 13. The influence of h and h_s on the velocity υ_o for $h_s=2$ m (red), 4 m (green), and 6 m (blue)
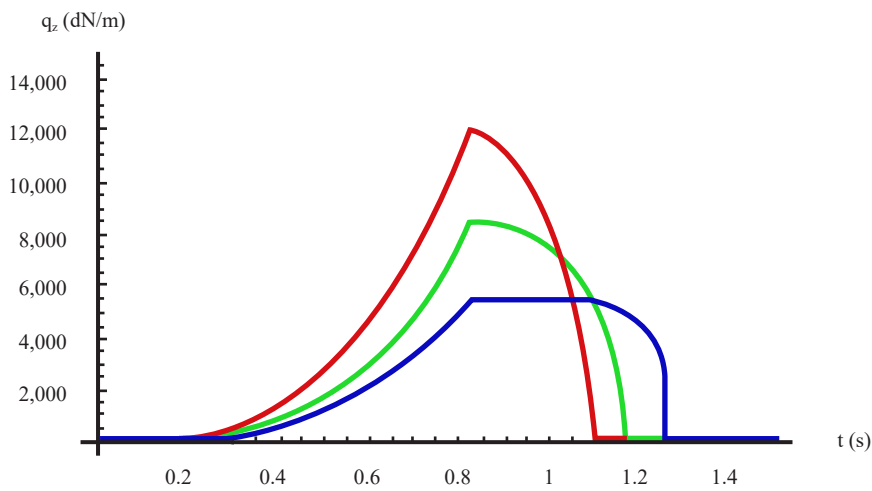

Figure 14. The influence of velocity υ_o on the vertical loading q_z: red curve $\upsilon_o = 11$ m/s, green curve $\upsilon_o = 9$ m/s, and blue curve $\upsilon_o = 7$ m/s, for $h_{cr} = 12$ m

7.2.3 Velocity and loads

In Figure 14, the influence of velocity v_o on the developing vertical loading q_z for constant $h_{cr} = 12$ m is shown. We observe that for a lower velocity, the loading decreases while the influence time increases.

7.3 The motion of the deck

For the results that follow, and in order to study the deck's motion, we use the following data: $h_o = 6$ m, $h_s = 2$ m, $b = 3$ m and $a = 5$ m; from Eq. (5) we find that $h_{cr} = 12.45$ m, while from Eq. (2) we get $v_o = 12.02$ m/s. We also assume that the form of the wave is expressed by $L_1 = L_2 = 4$ m.

7.3.1 Bridge of L = 16 m
(a) Vertical motion

Applying the relations of subsection 5.2, we obtain the plot in Figure 16. The maximum deformation found is max $w = 0.0972$ m at $t = 0.89$ s, i.e., $\dfrac{L}{164} > \dfrac{L}{250} = 0.064$ m. This deformation is unacceptable.
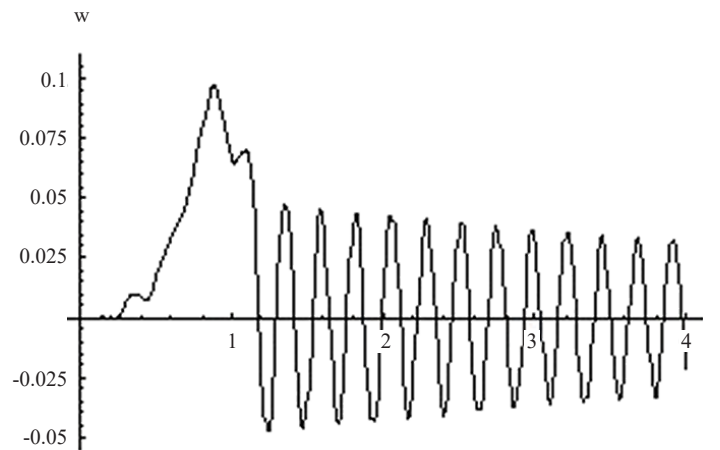

Figure 16. The vertical motion of the bridge of $L = 16$ m
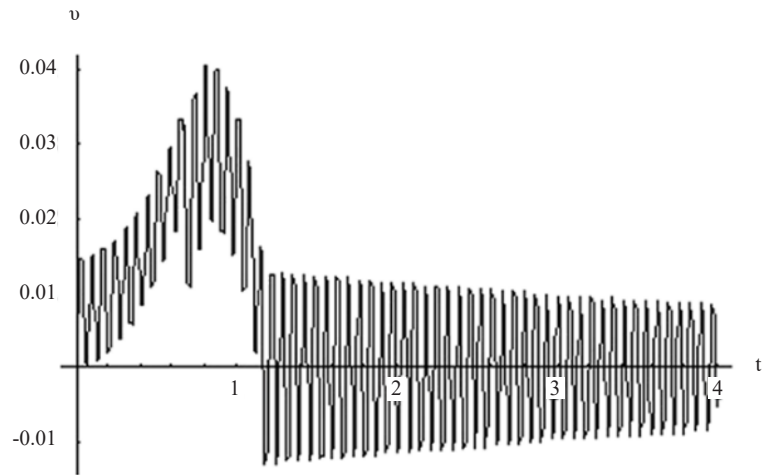
(b) Lateral motion

Applying the relations of subsection 5.3, we obtain the plot in Figure 17. The maximum deformation is max $v = 0.0404$ m at $t = 0.81$ s, i.e., $\dfrac{L}{395} < \dfrac{L}{250} = 0.0404$ m. This deformation is acceptable.
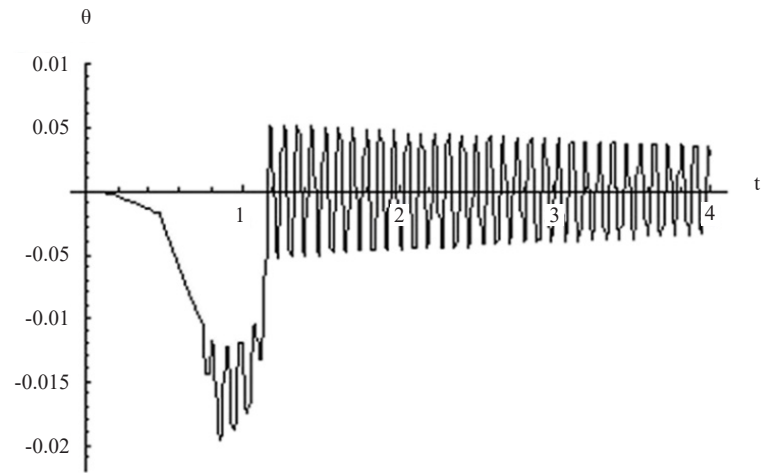
(c) Torsional motion

The time series of this motion (θ, t) are depicted in Figure 18. The maximum deformation is max $\theta = 0.0198$ rad at $t = 0.862$ s, i.e., $\theta = 1.15$ °, or 0.07 °/m. The acceptable torsion per unit length is 0.25 °/m.
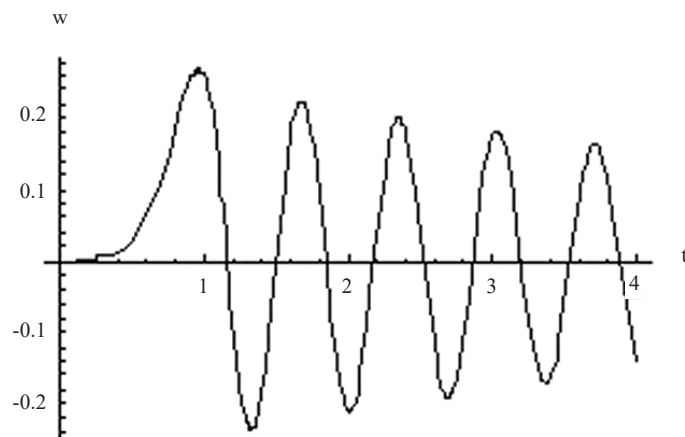
7.3.2 Bridge of L = 70 m

In the same manner as in the previous paragraph, we determine the dynamics of this particular bridge. The results for the vertical, lateral, and torsional motions are given in Figures 19, 20, and 21, respectively.
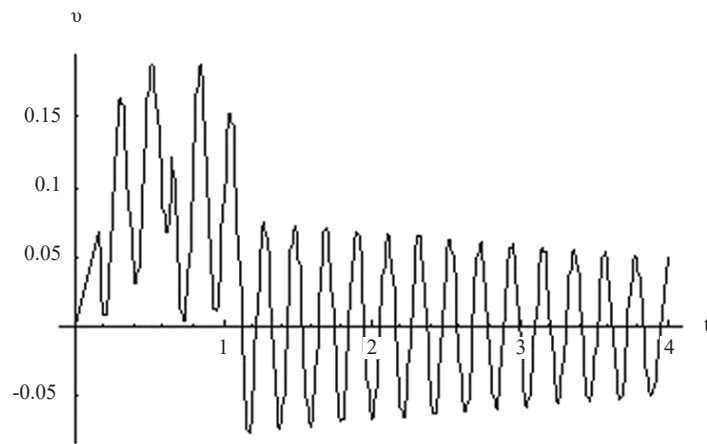
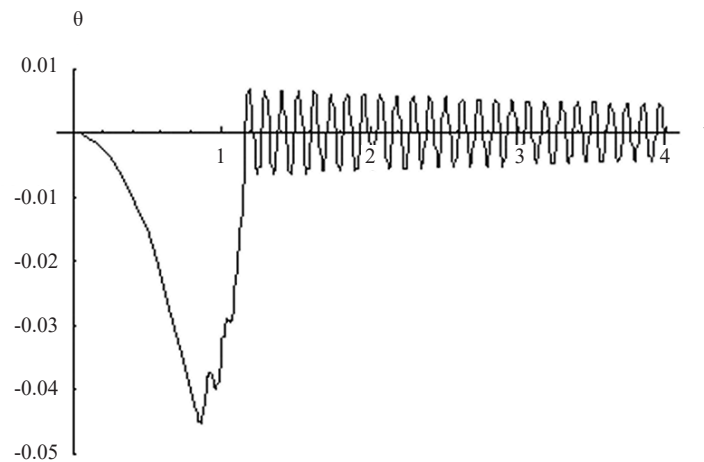**Figure 17.** The lateral motion of the bridge of $L = 16$ m

Figure 18. The torsional motion of the bridge of $L = 16$ m

Figure 19. The vertical motion of the bridge of $L = 70$ m

Figure 20. The lateral motion of the bridge of $L = 70$ m

Figure 21. The torsional motion of the bridge of $L = 70$ m

For the vertical dynamics, the maximum deflection is max $w = 0.272$ m at $t = 0.96$ s, and since $\dfrac{L}{257} < \dfrac{L}{250} = 0.28$ m, this deformation is acceptable.

For the lateral motion, it is found that max $v = 0.188$ m at $t = 0.845$ s, i.e., $\dfrac{L}{372} < \dfrac{L}{250} = 0.28$ m. This deformation is also acceptable.

As far as the torsional dynamics are concerned, the results obtained show that the maximum deformation is max θ = 0.045 m at $t = 0.865$ s, i.e., $\theta = 2.8°$ or 0.04 degrees/m. If the acceptable torsion per unit length is 0.25 degrees/m, then the deformation found is also acceptable.

7.4 *Bridge safety*
7.4.1 *Bridge of L = 16 m*
(a) *The rocking phenomenon*

For a closed cross-section the acting force is $F_b = 2 \times 5 \times 1 \times 16 \times 1{,}000 = 160{,}000$ daN. For an open cross-section (like the one in Figure 12) and with $H = 4$ m, we get:

$$h = \dfrac{\left(\dfrac{10,000}{1,000} + 0.5 + 4\right) - \sqrt{\left(\dfrac{10,000}{1,000} + 0.5 + 4\right)^2 - 2 \cdot 4 \cdot 1}}{2} = 0.139 \text{ m}$$

Acting force: $F_b = 2 \times 5 \times (0.5 - 0.139) \times 1,000 \times 16 = 59,200$ daN
Reacting forces: $F_{br} = 300 \times 10 \times 16 = 48,000$ daN
$\qquad\qquad F_{bt} = 2 \times 4 \times \pi \times 5,000 = 125,663$ daN
Evidently, $F_{br} + F_{bt} > F_b$, which means that the bridge is safe against the rocking phenomenon.

(b) *The shifting phenomenon*

Acting force: $F_h = (1,000/10) \times 1 \times 12^2 \times 16 = 230,400$ daN
Reacting forces: $F_{bs} = 2 \times 4 \times \pi \times 4,000 = 100,530$ daN
$\qquad\qquad F_{bf} = 0.150 \times 300 \times 10 \times 16 = 7,200$ daN

The inertia reacting forces are determined by the relation $F_{bi} = \displaystyle\int_0^L m\ddot{u}\, dx$, while the acting forces have a duration of at least $(L_1 + L_2)/v_o = 0.67$ s. From the diagram in Figure 22, we observe that the inertia forces react up to $t = 0.014$ s. Therefore, in our opinion, all the reacting forces cannot prevent the shifting phenomenon.
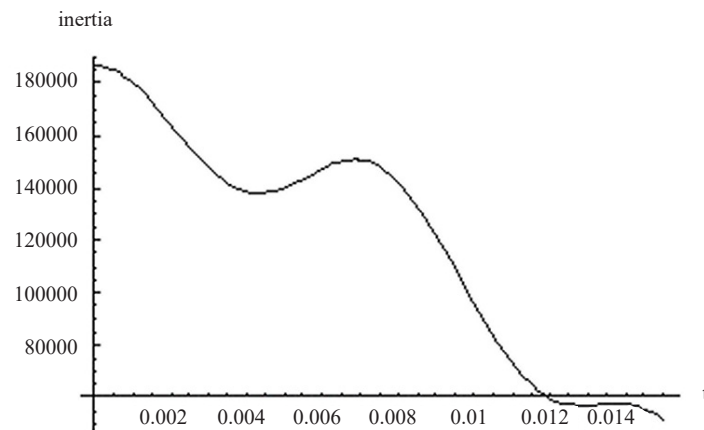

Figure 22. The inertia forces of the bridge of $L = 16$ m

(c) *The overturning phenomenon*

Acting moments: $m_b = F_h \times \dfrac{b}{2} = \dfrac{\gamma}{g} \times b \times L \times v_o^2 \times \dfrac{b}{2} = 115,200$ daNm
Reacting moments: $m_{s1} = mgLa = 300 \times 10 \times 16 \times 5 = 240,000$ daNm
$\qquad\qquad m_{s2} = 2 \times 2 \times \dfrac{\pi \cdot 2^2}{4} \times 5,000 \times 10 = 628,319$ daNm
It is readily perceived that $m_{s1} + m_{s2} > m_b$, i.e., the bridge is safe against the overturning phenomenon.

7.4.2 *Bridge of L = 70 m*
(a) *The rocking phenomenon*

For a closed cross - section the acting force is $F_b = 2 \times 5 \times 3 \times 70 \times 1,000 = 2,100,000$ daN. For an open cross-section (like the one of Figure 12) and with $H = 4$ m, we get:

$$h = \frac{\left(\dfrac{10,000}{1,000}+1.5+4\right) - \sqrt{\left(\dfrac{10,000}{1,000}+1.5+4\right)^2 - 2\cdot3\cdot4}}{2} = 0.397 \text{ m}$$

Acting force: $F_b = 2 \times 5 \times (1.5 - 0.397) \times 1,000 \times 70 = 777,100$ daN

Reacting forces: $F_{br} = 800 \times 10 \times 70 = 560,000$ daN

$F_{bt} = 2 \times 4 \times \pi \times 5,000 = 125,663$ daN

Here, $F_{br} + F_{bt} < F_b$, which means that the reacting forces cannot prevent the rocking phenomenon.

(b) *The shifting phenomenon*

Acting force: $F_h = (1,000/10) \times 3 \times 12^2 \times 70 = 3,024,000$ daN

Reacting forces: $F_{bs} = 2 \times 4 \times \pi \times 4,000 = 100,530$ daN

$F_{bf} = 0.150 \times 800 \times 10 \times 70 = 84,000$ daN

The inertia reacting forces are determined by the relation $F_{bi} = \int_0^L m\ddot{u}\,dx$ and shown in the plot in Figure 23. We observe that the reacting forces, even with the aid of the inertia ones, are smaller than the acting forces. Therefore, the shifting will occur.
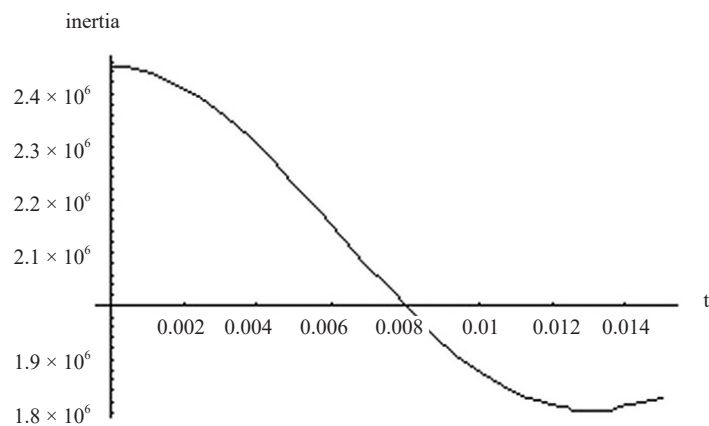

Figure 23. The inertia forces of the bridge of $L = 70$ m

(c) *The overturning phenomenon*

Acting moments: $m_b = \left(\dfrac{1,000}{10}\right) \times 3 \times 70 \times 12^2 \times \left(\dfrac{3}{2}\right) = 4,536,000$ daNm

Reacting moments: $m_{s2} = 2 \times 2 \times \dfrac{\pi \cdot 2^2}{4} \times 5,000 \times 10 = 628,319$ daNm

Here, $m_{s1} + m_{s2} < m_b$, i.e., the bridge is not safe against the overturning phenomenon.

Overall, the various situations related to the safety of both bridges are summarized in the contents of Tables 2 and 3.

8. Quantitative comparison with existing results obtained from numerical simulations

From the contents of the relevant referenced works regarding numerical simulations of the extreme flood action (summarized in the Introduction), objective difficulties arise for such a comparison, due to the following two facts:

(a) The simulations of the cited papers are not all alike, and in some cases, they differ significantly from each other.

(b) The characteristics of the exemplary bridge types (cross-section, material, height above sea level, length, and support conditions) used in this paper are by far different from the corresponding ones of the simulated bridge structures.

Hence, for a proper global quantitative comparison, all input and output data of the numerical simulations should be available, and those in return, should be adequately manipulated (calibration, scaling, etc.). This is rather impossible. Perhaps the use of the simulated bridge superstructures' characteristics (if acquired) could be used for further analysis within this work, but this again relies beyond its scope.

However, one may perceive that the results obtained herein, as far as the order of magnitude of the wave loads agrees satisfactorily for typical practical needs, with those ones of [23].

Moreover, using the data of [20], the diagram of Figure 24 is plotted, which exhibits again an acceptable level of approximation -for practical applications- to the results of Figure 14, in terms of the maximum value of the wave load.

Table 2. Decks without or with weak connections

Bridge Length (m)	16	70
Phenomenon	Safety Features	
Rocking	Not safe	Not safe
Shifting	Not safe	Not safe
Overturning	Safe	Not safe

Table 3. Decks connected to bearings

Bridge Length (m)	16	70
Phenomenon	Safety Features	
Rocking	Safe	Not safe
Shifting	Not safe	Not safe
Overturning	Safe	Not safe
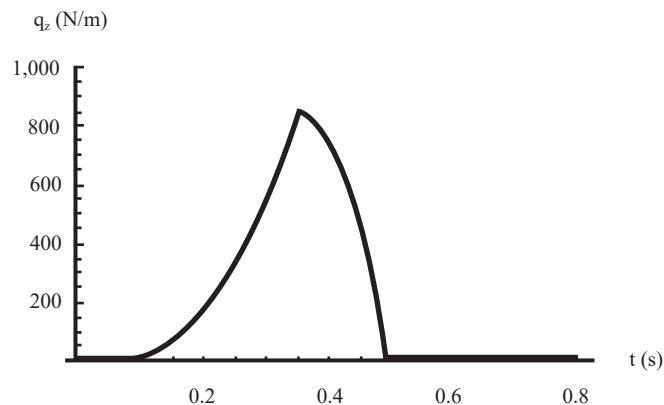
Figure 24. The wave load with data from reference [20]

9. Conclusions

This study presents a simple mathematical model based on simple hydraulic principles for the preliminary design of bridges to be constructed in tsunami-prone locations, in order to avoid rigorous analysis using ocean and coastal engineering.

The results in terms of values and duration of the acting waves are in satisfactory agreement with existing experimental and theoretical studies.

This study has two parts. One deals with the deformation of the deck and the other with the safety of the entire bridge. In the former, we test the deck's ability to withstand loads from a tsunami provided that it is stably joined to the bearings.

Based on the representative small and long bridges' models analyzed herein, the following conclusions can be drawn:

• From this first part, we observe that the vertical deformations of small bridges are not acceptable, while those of long bridges are close to or slightly larger than the acceptable limits of deformations. Both small and long bridges are safe concerning the lateral as well as the torsional deformations.

• Although decks are usually not connected to their bearings, only rest on them without any other connection, we assume that both small and long bridges are connected to their bearings by a couple of bolts.

• We note that, for small bridges with a smaller deck width, the reacting moments due to the dead weight of the deck and the reaction of the bolts are smaller and therefore, the bridge may not be able to prevent the overturning phenomenon.

• The proposed scheme, although based on certain simplifications and assumptions, manages to capture the salient features of the phenomena dealt with, in terms of tsunami actions, developing generalized forces, bridge dynamic response, and safety issues.

Conflict of interest

The authors declare no competing financial interest.

References

[1] A. Zerva, "Response of multi-span beams to spatially incoherent seismic ground motions," *Earthquake Engineering & Structural Dynamics*, vol. 19, no. 6, pp. 819-832, 1990.

[2] T. E. Price and M. O. Eberhard, "Effects of spatially varying ground motions on short bridges," *Journal of Structural Engineering*, vol. 124, no. 8, pp. 948-955, 1998.

[3] G.T. Michaltsos and I. G. Raftoyiannis, "A mathematical model for rocking, overturning and shifting problems in bridges," *Engineering Structures*, vol. 30, no. 12, pp. 3587-3594, 2008.

[4] W. Xiong, C. S. Cai, K. Byeongseo, and J. S. Ye, "Overturning-collapse modeling and safety assessment or bridges supported by single-column piers," *Journal of Bridge Engineering*, vol. 22, no. 11, pp. 1-13, 2017.

[5] T. F. Deng, J. P. Zhang, S. Li, and Y. Wang, "Anti-overturning stability coefficient of curved girder bridges considering seismic action," *Journal of Vibroengineering*, vol. 21, no. 3, pp. 710-725, 2019.

[6] V. G. Panchang and D. Li, "Large waves in the gulf of Mexico caused by Hurricane Ivan," *Bulletin of the American Meteorological Society*, vol. 87, no. 4, pp. 481-489, 2006.

[7] K. Kosa, "Damage analysis of bridges affected by Tsunami in the Great East Japan Earthquake," *Journal Society of Civil Engineers*, vol. 2, no. 1, pp. 77-93, 2014.

[8] S. C. Yim, K. F. Cheung, M. J. Olsen, and Y. Yamazaki, "Tohoku Tsunami Survey, Modeling and Probabilistic Load Estimation Applications," in Proceedings of the International Symposium on Engineering Lessons Learned from the 2011 Great East Japan Earthquake, 2012, Tokyo, Japan, 430-443.

[9] M. Azadbakht and S. C. Yim, "Simulation and estimation of tsunami loads on bridge superstructures," *Journal of Waterway, Port, Costal and Ocean Engineering*, vol. 141, no. 2, 04014031, 2015.

[10] T. Xiang, D. Istrati, S. C. Yim, I. G. Buckle, and O. Lomonaco, "Tsunami loads on a representative coastal bridge

deck: Experimental study and validation of design equations," *Journal of Waterway, Port, Costal and Ocean Engineering*, vol. 146, no. 5, 04020022, 2020.

[11] H. R. Riggs, I. N. Robertson, K. F. Cheung, G. Pawlak, Y. L. Young, and S. C. Yim, "Experimental simulation of tsunami hazards to buildings and bridges," Proceedings of 2008 NSF Engineering Research and Innovation Conference, Knoxville, Tennessee, USA, 2008, pp. 1056-1064.

[12] S. Araki and I. Deguchi, "Experimental study on tsunami fluid force on bridge across narrow river," In Proceedings of the 5th International Conference on Asian and Pacific Coasts, 2010, pp. 143-150.

[13] B. E. Larsen, L. K. Arbøll, S. F. Kristoffersen, S. Carstensen, and D. R. Fuhrman, "Experimental study of tsunami-induced scour around a monopile foundation," *Coastal Engineering*, vol. 138, pp. 9-21, 2018.

[14] S. Istrati, I. Buckle, P. Lomonaco, and S. C. Yim, "Deciphering the tsunami wave impact and associated connection forces in open-girder coastal bridges," *Journal of Marine Science and Engineering*, vol. 6, no. 4, p. 148, 2018.

[15] C. E. Synolakis, "Tsunami runup on steep slopes - How hood linear theory really is," *Tsunami Hazard*, vol. 4, no. 2, pp. 221-234, 1991.

[16] E. N. Pelinovsky and R. K. Mazova, "Exact analytical solutions of nonlinear problems of tsunami wave run-up on slopes with different profiles," *Natural Hazards*, vol. 6, no. 3, pp. 227-249, 1992.

[17] K. Goto, O. Fujiwara, and S. Fujino, "Thematic section: Bridging the gap separating geological studies and disaster mitigation countermeasures for earthquakes and tsunami," *Island Arc*, vol. 19, no. 3, pp. 371-373, 2010.

[18] J. D. Bricker and A. Nakayama, "Contribution of trapped air, deck superelevation, and nearby structures to bridge deck failure during a tsunami," *Journal of Hydraulic Engineering*, vol. 140, no. 5, 05014002, 2014.

[19] F. Greco, P. Lonetti, and P. N. Blasi, "Vulnerability analysis of bridge superstructures under extreme fluid actions," *Journal of Fluids and Structures*, vol. 93, no. 409, 102843, 2020.

[20] F. Greco, P. Lonetti, and P. N. Blasi, "Impact mitigation measures for bridges under extreme flood actions," *Journal of Fluids and Structures*, vol. 106, 103381, 2021.

[21] A. De Rosis, "A lattice Boltzmann-finite element model for two-dimensional fluid-structure interaction problems involving shallow waters," *Advances in Water Resources*, vol. 65, pp. 18-24, 2014.

[22] H. Salem, S. Mohssen, K. Kosa, and A. Hosoda, "Collapse analysis of utatsu ohashi bridge damaged by tohuku tsunami using applied element method," *Journal of Advanced Concrete Technology*, vol. 12, no. 10, pp. 388-402, 2014.

[23] N. Ataei and J. E. Padgett, "Influential fluid-structure interaction modelling parameters on the response of bridges vulnerable to coastal storms," *Structure and Infrastructure Engineering*, vol. 11, no. 3, pp. 321-333, 2015.

[24] Y. Huang and C. Zhu, "Numerical analysis of tsunami-structure interaction using a modified MPS method," *Natural Hazards*, vol. 75, no. 3, pp. 2847-2862, 2015.

[25] E. M. Sosa, J. C.-S. Wong, A. Adumitroaie, E. J. Barbero, and G. J. Thompson, "Finite element simulation of deployment of large-scale confined inflatable structures," *Thin-Walled Structures*, vol. 104, pp. 152-167, 2016.

[26] M. J. Zhu, I. Elkhetali, and, M. H. Scott, "Validation of opensees for tsunami loading on bridge superstructures," *Journal of Bridge Engineering*, vol. 23, no. 4, 04018015, 2018.

[27] S. L. Douglass, S. A. Hughes, S. Rogers, and Q. Chen, "The impact of Hurricane Ivan on the coastal roads of Florida and Alabama: A preliminary report," Report to Coastal Transportation Engineering Research and Education Center, University of South Alabama, Mobile, AL 2014, pp. 19.

[28] S. L. Douglass, Q. Chen, J. M. Olsen, B. L. Edge, and D. Brawn, "Wave forces on bridge decks", University of South Alabama, Coastal Transportation Engineering Research and Education Center, University of South Alabama, Mobile, AL, 2006, pp. 74.

[29] I. N. Robertson, S. C. Yim, H. R. Riggs, and Y .L. Young, "Costal Bridge Performance During Hurricane Katrina", Third International Conference on Structural Engineering, Mechanics and Computation, Cape Town, South Africa, Millpress, Rotterdam, Netherlands, 2007, pp. 1864-1870.

[30] K. Maruyama, Y. Tanaka, K. Kosa, A. Hosoda, N. Mizutami, and T. Nakaimura, "Evaluation of Tsunami Force Acted on Bridges by Great East Japan Earthquake", In 10th International Conference on Urban Earthquake Engineering, 2013, pp. 7-16.

[31] M. Akiyama and D. M. Frangopol, "Reliability of Bridges under Seismic and Tsunami Hazards," In Vulnerability, Uncertainty, and Risk: Qualification, Mitigation, and Management, Liverpool, UK, 2014.

[32] A. K. Alhamid, M. Akiyama, H. Ishibashi, K. Aoki, S. Koshimura, and D. M. Frangopol, "Framework for probabilistic tsunami hazard assessment considering the effects of sea-level rise due to climate change," *Structural Safety*, vol. 94, 102152, 2022.

[33] EN 1991-1-6: 2005, §4.9 "Actions caused by waters-water effects caused by an earthquake-tsunamis".

[34] ASCE-SEI-7-16, "Minimum Design Loads and Associated Criteria for Buildings and Other Structures," American Society of Civil Engineers, 2017.

[35] FEMA P-646; "Guidelines for Design of Structures for Vertical Evacuation from Tsunamis" Applied Technology Council, Redwood City, California 94065, August 2019,

[36] D. Istrati and I. G. Buckle, "Tsunami Loads on Straight and Skewed Bridges - Part I: Experimental Investigation and Design Recommendations," University of Nevada, Reno (Oregon Department of Transportation) Report FHWA-OR-RD-21-12, February 2021.

[37] D. Istrati and I. G. Buckle, "Tsunami Loads on Straight and Skewed Bridges - Part 2: Numerical Investigation and Design Recommendations, University of Nevada, Reno (Oregon Department of Transportation) report FHWA-OR-RD-21-13, March 2021.

[38] Th. Karambas, I. Krestenitis, and X. Koutitas, *Elements of wave engineering*, Kallipos Ed., Thessaloniki (in Greek), 2015.

Appendix

A1. *Impact of a water vein on a flat vertical surface*

Let us consider the water vein of Figure A1, which has a cross-section of area f and impacts on the flat surface of a plate S. The developed pressure F and the reaction P are:

$$F = P = \rho \cdot Q \cdot v = \frac{\gamma}{g} \cdot f \cdot v^2 \qquad (A1)$$

where v is the velocity of the vein and Q is the water supply. For a plate moving with a velocity v_p in the same direction as the water vein, the volume of water impacting the plate is $Q_p = f \cdot (v - v_p)$ and the developed pressure becomes

$$F = \frac{\gamma}{g} \cdot f \cdot (v - v_p)^2 \qquad (A2)$$

The produced work per unit time is

$$\mathcal{E} = F \cdot v_p = \frac{\gamma}{g} \cdot f \cdot (v - v_2)^2 \cdot v_p \qquad (A3)$$

Becoming the maximum when $\dfrac{d\mathcal{E}}{dv_p} = 0$, leading to

$$v_p = \frac{v}{3} \text{ or } v_p = 0 \qquad (A4)$$

For $v_p = 0$, there is no impact; hence, for $v_p = \dfrac{v}{3}$, we get

$$\mathcal{E}_{max} = \frac{4}{27} \cdot \frac{\gamma \cdot v^3}{g} \qquad (A5)$$
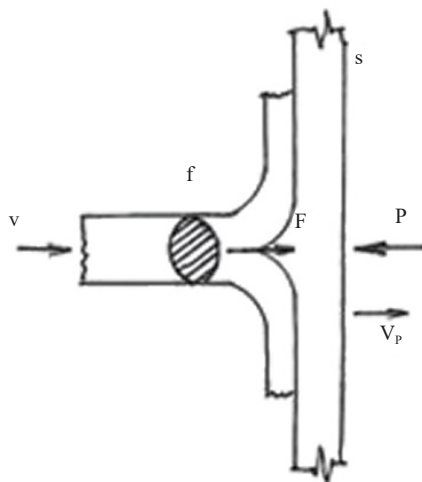

Figure A1. Impact of a water vein on a vertical flat plate

A2. *Impact of a water vein on a flat inclined surface*

We consider that the flat plate is inclined by an angle φ with respect to the direction of the water vein, as illustrated in Figure A2.
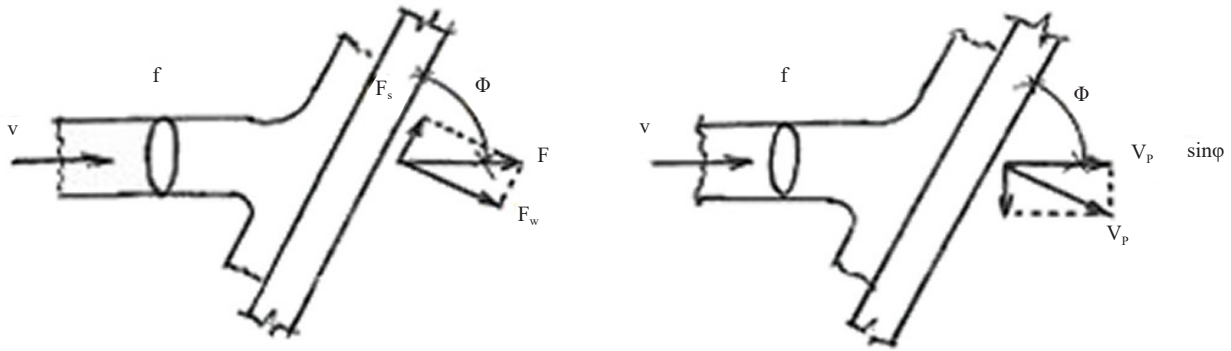

Figure A2. Impact of a water vein on an inclined flat plate

In the same manner as in Section A1, we may write that

$$F = \frac{\gamma}{g} \cdot f \cdot v^2 \tag{A6}$$

$$F_w = \frac{\gamma}{g} \cdot f \cdot v^2 \cdot sin\varphi \tag{A7}$$

$$F_s = \frac{\gamma}{g} \cdot f \cdot v^2 \cdot cos\varphi \tag{A8}$$

For a plate that moves with velocity v_p, perpendicular to its surface, we determine that the volume of water impacting the plate is equal to $Q_p = f \cdot (v - v_p \cdot sin\varphi)$ and the developed pressure will be $F = \frac{\gamma}{g} \cdot Q_p \cdot (v - v_p \cdot sin\varphi) = \frac{\gamma}{g} \cdot (v - v_p \cdot sin\varphi)^2$. Hence,

$$F_w = \frac{\gamma}{g} \cdot f \cdot (v - v_p \cdot sin\varphi)^2 \cdot sin\varphi \tag{A9}$$

$$F_s = \frac{\gamma}{g} \cdot f \cdot (v - v_p \cdot sin\varphi)^2 \cdot cos\varphi \tag{A10}$$

A3. *Fall of a water vein*

A water vein is launched from a height h with a horizontal velocity v_o. The motion that occurs is that of an initially horizontal shot. According to the principle of independence of movements, the duration of the water drop until it reaches the ground depends on the height h. Evidently, the landing distance s of the vein, as shown in Figure A3, depends on

the launch velocity v_o, i.e., $s = v_o \cdot \sqrt{\dfrac{2 \cdot h}{g}}$. Since the final vertical speed is easily calculated as $v_h = g \cdot t = \sqrt{2 \cdot h \cdot g}$, the velocity of impact is $v = \sqrt{v_o^2 + 2 \cdot h \cdot g}$.
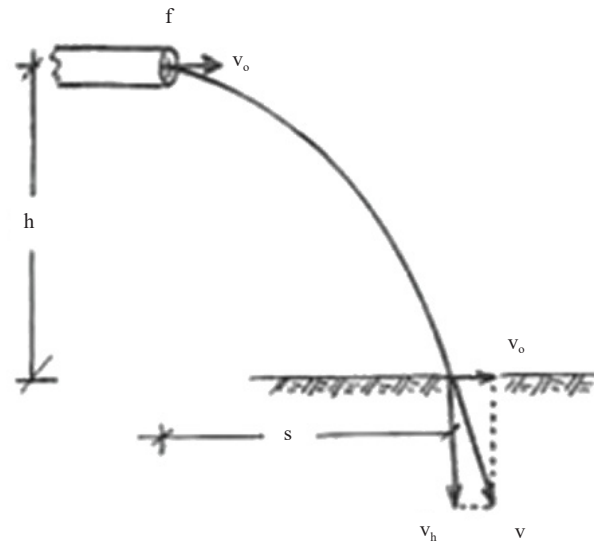
Figure A3. The drop of a water vein